UDC 551.558.21:551.511.6

Effects of Internal Gravity Waves on Energy Budgets and the Vertical Transport of Angular Momentum Over Mountainous Terrain

GENE L. WOOLDRIDGE—*Department of Soil Science and Biometeorology, Utah State University, Logan, Utah*

ABSTRACT—High-resolution pictures obtained with a handheld camera during the earth-orbiting photographic mission of the Apollo 9 spacecraft provided a unique opportunity to map the areal extent of gravity waves over the southwestern United States. The gravity waves were manifested in thin layers of middle- and high-cloud patterns over the rugged terrain of Arizona, Colorado, and New Mexico.

Zonal shearing stress gradients in stably stratified air flowing over rugged mountain terrain indicated very large subgrid-scale vertical fluxes of zonal momentum. Maximum stress values of several tens of dynes·cm^{-2} (10^{-3} mb) were calculated for the lower tropospheric layers where the air flowed over the high Rocky Mountains of central New Mexico. The vertical fluxes of zonal momentum were directed upward to tropopause levels when extensive areas of gravity waves covered eastern Arizona, New Mexico, and western Texas.

The potential energy contained in the wave population attained values through the troposphere as high as 9.3×10^5 J·m^{-2}; this potential energy was a substantial part of the atmospheric energy budget. The residual "dissipation" term in the kinetic energy budget indicated a subgrid-scale flux of energy downward from the lower stratosphere concurrent with the upward flux of zonal momentum in the troposphere. Atmospheric turbulence exhibited a maximum during the wave occurrence, diminishing gradually thereafter.

1. INTRODUCTION

The vertical transport of relative angular momentum determines in part the structure and contributes toward the maintenance of the atmospheric circulation (Palmén and Newton 1969). The large-scale mean vertical flux of relative angular momentum in middle latitudes has been measured for extended periods of time and has been found inadequate to satisfy the requirements of the atmosphere (Palmén 1966, Oort and Rasmusson 1970). Thus the vertical transport may be largely due to eddies on many scales, from the planetary wavelengths to small-scale shearing stresses (Reiter 1969).

Starr and Dickinson (1963) measured the vertical transport of relative angular momentum in large-scale vertical eddies; they found opposing signs of transport according to the seasons, with downward flux in January and upward flux in April. Lorenz (1967) suggested that the large-scale eddies were ineffective in bringing about the required vertical transport of relative angular momentum.

Calculations of the vertical eddy transport by various length scales led Gilman (1964) to conclude that the eddies on length scales below the conventional rawinsonde network may at times move momentum near tropopause levels in a direction vertically opposite to the flux due to larger scales. Measurements of "negative eddy viscosity" near the midlatitude jet stream were interpreted by Gilman as evidence that the net effect of vertical eddies of all scales near the jet brought about momentum transport into the jet stream.

As opposed to the down-gradient transport of momentum predicted by classical mixing-length theory whereby fluid motion is retarded in high-velocity regions, momentum may flow against the velocity gradient, increasing the velocity at jet stream levels. This transport of momentum against the gradient has been termed "negative viscosity" and has become the object of increasing interest during the past two decades (Starr 1968).

Kung (1967) also found "negative dissipation" near the tropopause in calculations of the annual mean kinetic energy budgets over North America. Jensen (1961) speculated that the negative dissipation, which he calculated at tropopause levels for January 1958, might be explained by a generation of kinetic energy in eddies on a scale undetected in the conventional meteorological data network.

The generation suggested by Jensen may not be required if energy flows vertically through a preferred mode of some atmospheric transport mechanism. The research reported here investigates the possibility that subgrid-scale gravity waves can redistribute energy vertically in sufficient quantity to account for this anomalous dissipation of energy.

The possibility of vertical fluxes of angular momentum on small scales in addition to synoptic and larger scales was suggested by Priestley (1967*a*). In an earlier discussion, Priestley (1967*b*) indicated that shearing stresses above the planetary boundary layer probably play a significant part in the general circulation of the atmosphere. These shearing stresses include (1) true viscous drag forces that dissipate heat and have an effect on a total atmospheric heat budget and (2) vertical eddy fluxes of momentum.

Westerly airflow crossing the mountainous southwestern United States often experiences an acceleration in

the upper troposphere and a sharpening of the vertical profile of zonal velocity (Rossby 1951). The vertical stability distribution apparently plays an important part in the concentration of zonal momentum in shallow layers of air, resulting in sharp jets.

Riehl and Baer (1964) showed that the western mountainous region of North America extending from 30° to 60° N contributed a large part of the vertical momentum exchange between the earth's surface and the atmosphere. They found that the resultant vertical flux of zonal relative momentum could take place either upward or downward. The mountain effect was also shown by Kung (1968) to be significant in momentum transport over the North American Continent.

The vertical transport of relative angular momentum from levels of low zonal velocities to levels of higher zonal velocities can not be explained through the action of cumulonimbus clouds that act to decrease the wind shear by vertical mass exchange. Moreover, there are extensive continental areas in winter over which no cumulonimbus clouds are to be found. It seems unlikely that convective turbulence in a stably stratified region can account for the necessary vertical redistribution of relative angular momentum over continents in winter (Palmén and Newton 1969).

2. DATA SOURCES AND THE REGION OF STUDY

The data required for the calculations of the shearing stresses consisted of the heights of the pressure surfaces, wind directions, and wind speeds. The conventional 0000 and 1200 GMT rawinsonde data were supplemented with 1800 GMT pilot balloon wind information and wind directions deduced from cloud streaks and streets in Apollo 9 photographs taken at approximately 1800 GMT.

The 1800 GMT computational time was chosen primarily to take advantage of the subsynoptic scale wind information recorded in the earth-oriented Apollo 9 pictures. Center differencing for 1800 GMT utilized the 1200 GMT data for the same day and the 0000 GMT data for the following day.

The presence of high, rugged terrain, the regular spacing of rawinsonde station locations, and the coverage by high-resolution Apollo 9 photography determined the region selected for study. The period of study encompassed the earth-oriented photographic mission of the Apollo crew. The area outlined in figure 1 in solid lines constituted the region, covering about 10^{12} m^2 in Arizona, New Mexico, and parts of western Texas and Oklahoma. Mountain peaks in eastern New Mexico rise to 4 km, with numerous elevations over 3 km in Arizona and New Mexico. The ridges are irregularly spaced and oriented, allowing interaction between the perturbations imposed on the airflow passing over the terrain. The frequent occurrence of clear air turbulence (Reiter and Foltz 1967) reflects the generation and interaction of mountain waves over the region. The region is also an area over which the jet stream is frequently located (Lester 1969).

Wind directions deduced from the orientation of cumulus streets and cirrus streaks in photographs taken with

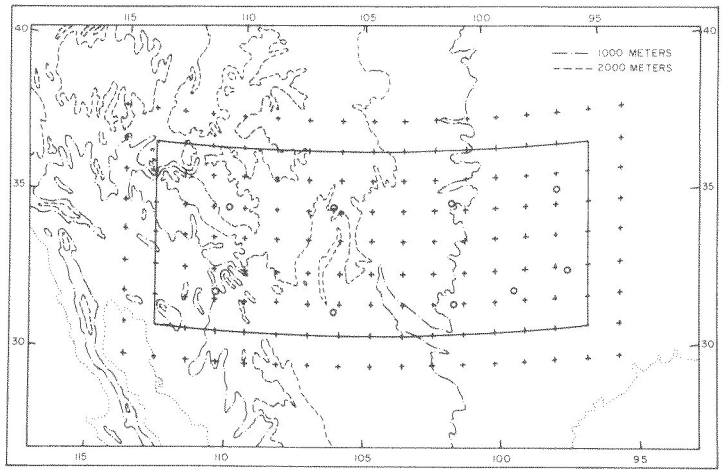

FIGURE 1.—Region of southwestern United States selected for application of stress and momentum relationships. Computational gridpoints and the computational area are indicated by crosses and solid lines, respectively. Circles are rawinsonde stations.

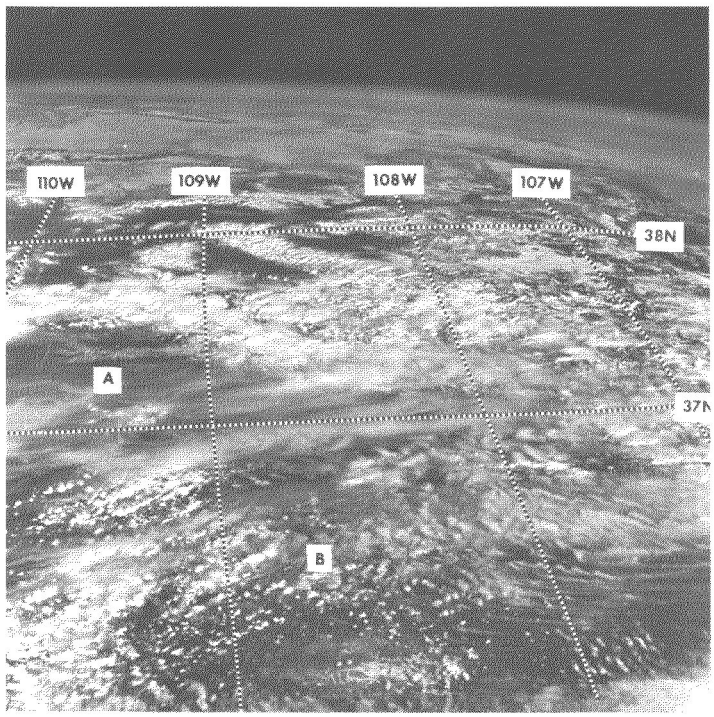

FIGURE 2.—Apollo 9 handheld camera photograph (No. 3443) taken at approximately 1804 GMT on Mar. 9, 1969. Long cumulus streets at about 12,000 ft MSL can be seen at B. Cirrus streaks are visible at A, extending eastward to 107°W, 37°N.

Apollo 9 handheld cameras augmented the data for 1800 GMT on Mar. 8–12, 1969. The cirrus streaks and cumulus streets like those in figure 2 at A and B, respectively, closely approximated the direction of air flow at cloud levels when compared to available pilot balloon data. Figure 3 indicates the 1800 GMT 500-mb wind data from rawinsondes, pilot balloons, and Apollo photographs on Mar. 9, 1969.

The extensive wave populations photographed with the Apollo 9 cameras indicated the presence of mesoscale gravity waves over a large portion of eastern Arizona,

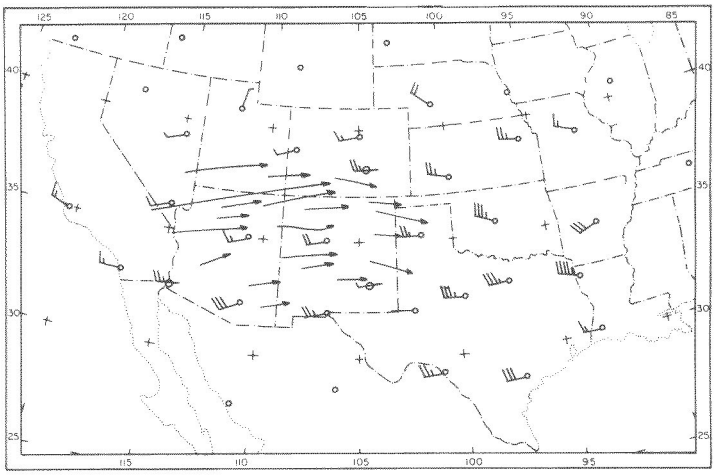

FIGURE 3.—Wind data used for objective analysis for 1800 GMT on Mar. 9, 1969, at the 500-mb level. Barbs indicate velocity in m/s. Indicators originating on stations are interpolated from rawinsonde data; those passing through stations are from pibals. Streaklines are derived from cloud streaks at 19,000–23,000 ft MSL.

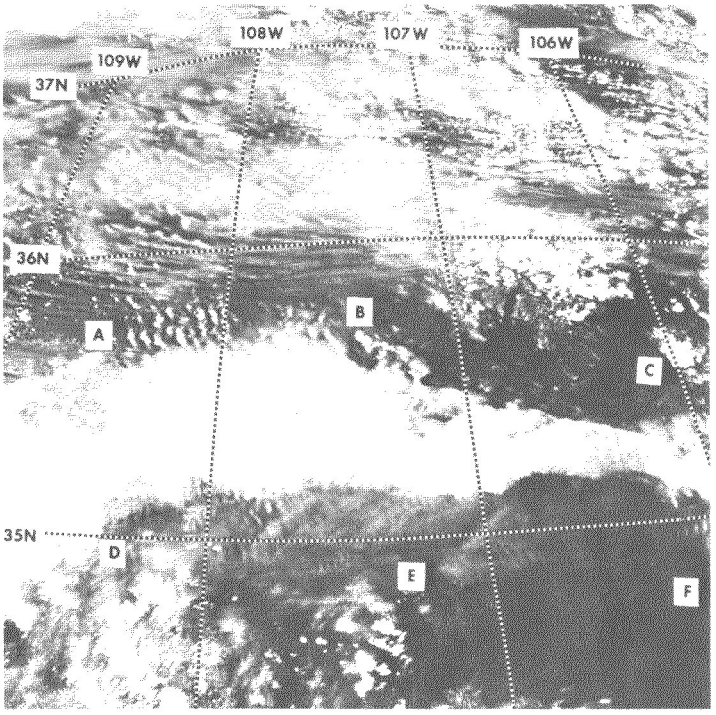

FIGURE 4.—Apollo 9 handheld camera photograph (No. 3441) taken at approximately 1804 GMT on Mar. 9, 1969. Cirrus streaks appear in the area north of B. The sharp cutoff from B to C coincides with the axis of the maximum wind at cloud level (about 500 mb).

New Mexico, and western Texas. These waves were manifested in the clouds at stable atmospheric layers near 500 and 700 mb on Mar. 9, 1969 (see fig. 4).

3. METHOD OF COMPUTATION

The Mar. 8–13, 1969, 0000 and 1200 GMT rawinsonde data for the nine stations within and for 16 stations surrounding the region were first reduced to u- and v-components. The time series of the standard pressure heights and wind components for each station were then subjected to a cubic "spline" curve fitting and interpolation technique to extract 1800 GMT data.

The spline procedure fits a smooth curve to a given set of points using normalized cubic polynomials; one cubic for each interval (Fowler and Wilson 1966). A third-degree polynomial is selected as the simplest expression that always exists and is not ambiguous. Translation and rotation of the coordinate axes accomplishes the normalization; only three coefficients must be found to describe each cubic polynomial.

The curve passes through each point in the series. This contrasts with the normal procedure in which the form of the fitted equation is predetermined and coefficients are chosen to pass the curve near the points. As each point is treated in turn, the slope of that point is adjusted until the adjacent normalized curves match their curvature. Thus, one obtains continuous position, slope, and curvature along the curve.

The spline procedure preserves the initial roughness of the data series. A prescribed fractional movement of points along the curve serves to remove local roughness, resulting in a new cubic spline. This method may be iterated until the desired smoothness of the curve is attained.

The total wind data population from the rawinsonde time series, cloud streets and streaks on the Apollo 9 photographs, and pilot balloons was objectively fitted to the grid shown in figure 1. The longitudinal grid line is true at 104°30′ W, and the grid lengths are 1.111×10^5 m (one latitude degree) in the x- and y-directions; the x-direction lies along latitude lines. This 1° grid network yielded a 2° distance interval for center differencing in horizontal space.

Grid-fitting was accomplished at 100-, 150-, 200-, 300-, 400-, 500-, and 700-mb levels by a two-dimensional cubic spline technique similar to one developed by Fritsch (1969). The cubic curve calculation for the one-dimensional spline was replaced with a spherical surface calculation for the two-dimensional spline from which data was extracted for gridpoints on a surface; the surface was represented by spherical surfaces spliced at a discrete number of points.

Pressure heights interpolated from the time series by the one-dimensional spline were subjectively analyzed. Computations were performed for the standard levels at which wind data were fitted, assuming atmospheric layers centered on these levels. Layer thicknesses ranged from 50 mb at the upper level to 175 mb for the 700-mb level.

4. SYNOPTIC SITUATION

The 300-mb 1800 GMT interpolated pressure-height contour (figs. 5A–5C) and zonal wind isotach (figs. 6A–6C) analyses for Mar. 8–10, 1969, indicate the nature of the upper tropospheric flow. Sustained high-velocity zonal winds characterized this period of time over which the calculations extended. The fixed computational grid location was chosen to take advantage of good rawinsonde coverage, to contain the consistently high-velocity winds,

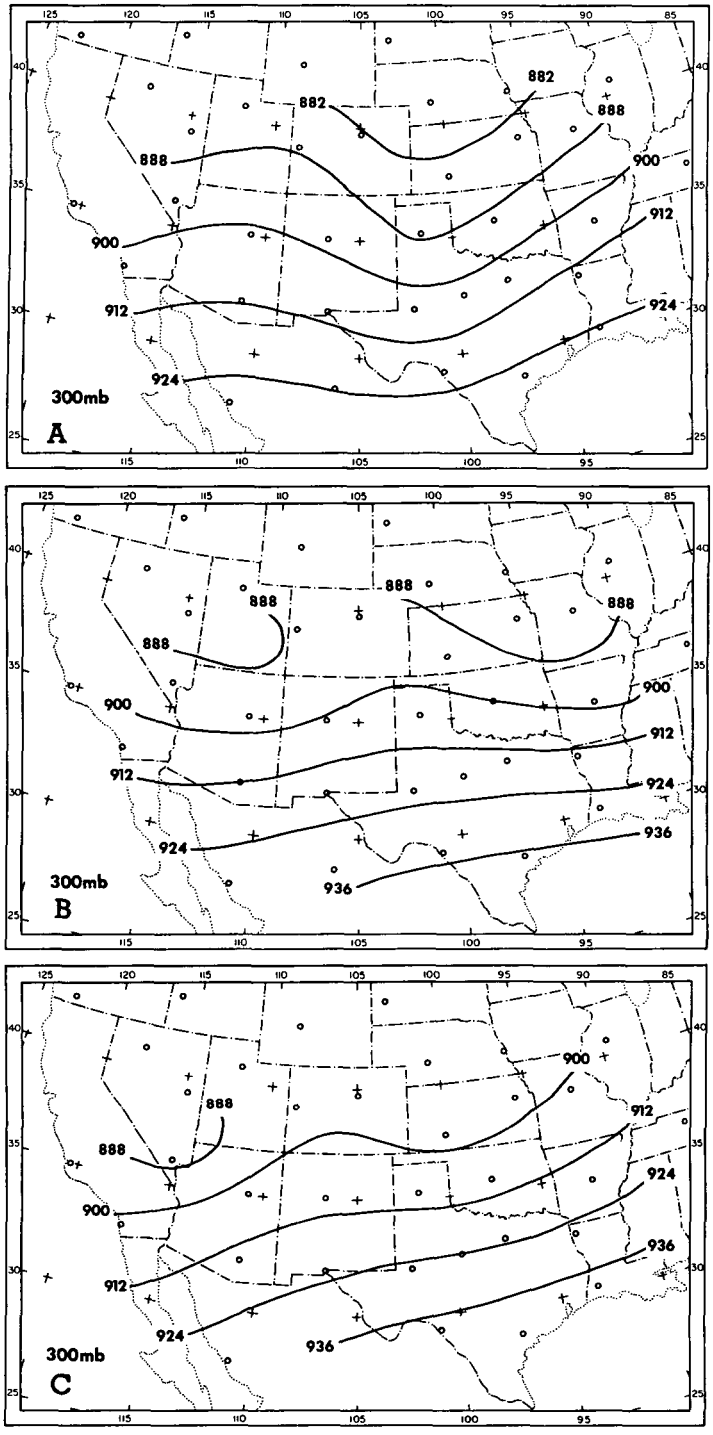

FIGURE 5.—Height contours in dekameters (dam) for 1800 GMT on (A) Mar. 8, (B) Mar. 9, and (C) Mar. 10, 1969, interpolated 300-mb maps.

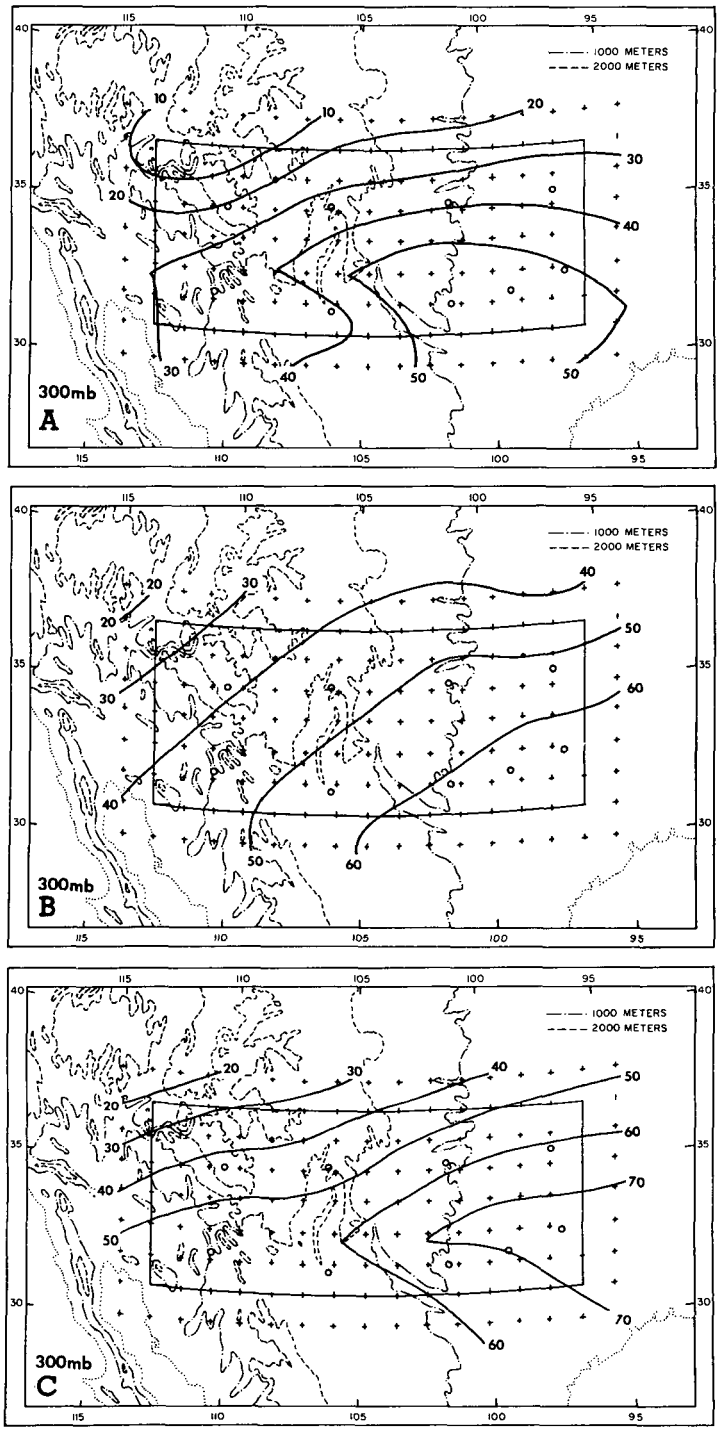

FIGURE 6.—Isotachs of zonal wind in m/s for 1800 GMT on (A) Mar. 8, (B) Mar. 9, and (C) Mar. 10, 1969, interpolated 300-mb maps.

and to cover the rugged terrain of Arizona and New Mexico.

5. ZONAL STRESSES AND ANGULAR MOMENTUM

The absolute angular momentum of a parcel of air can be expressed as

$$M=\Omega a^2 \cos^2 \phi + ua \cos \phi \qquad (1)$$

where M is the absolute angular momentum, Ω is the angular rotation rate of the earth about its axis, a is the mean radius of the earth, ϕ is the latitude, and u is the wind velocity along a latitude circle. The first term on the right-hand side of eq (1) represents the contribution due to the earth's rotation; the second term is due to the motion of the atmosphere relative to the earth's surface.

The angular momentum of the atmosphere changes through the action of pressure torque and friction torque

according to

$$\frac{dM}{dt}=\frac{-r}{\rho}\frac{\partial p}{\partial x}+rF_x \tag{2}$$

per unit mass, where $r=a\cos\phi$, ρ is the atmospheric density, $\partial p/\partial x$ is the pressure gradient due to differences in zonal pressure across the region of study, and F_x is the frictional force exerted by shearing stress gradients in the free atmosphere or by frictional "drag" at the earth-atmosphere interface.

The two-dimensional shearing stress force per unit mass, $\mathbf{F}_2$, may be expressed (Haurwitz 1941) as

$$\mathbf{F}_2=F_x\mathbf{i}+F_y\mathbf{j} \tag{3}$$

in which $\mathbf{i}$ and $\mathbf{j}$ are unit vectors. The stress forces are

$$F_x=-g\frac{\partial\tau_x}{\partial p} \tag{4}$$

and

$$F_y=-g\frac{\partial\tau_y}{\partial p} \tag{5}$$

through the assumption of hydrostatic equilibrium, where τ_x and τ_y are the zonal and meridional stress components, respectively.

The stress force components can be introduced into the equations for horizontal motion, in the pressure coordinate system, after dropping second-order terms. This gives

$$-g\frac{\partial\tau_x}{\partial p}=\frac{du}{dt}-fv+g\frac{\partial z}{\partial x} \tag{6}$$

and

$$-g\frac{\partial\tau_y}{\partial p}=\frac{dv}{dt}+fu+g\frac{\partial z}{\partial y}. \tag{7}$$

In cases of air flow at or near jet stream levels, the accelerations and gradients encountered require this inclusion of the inertial terms du/dt and dv/dt; v is the wind velocity along the meridians.

The vertical stress gradients were computed as residuals using eq (6) and (7) with the three-dimensional Eulerian form for du/dt and dv/dt and under the assumption that vertical velocity $\omega=0$ at 75 mb, the top of the volume. Simple center differencing was used for time and space increments.

Figure 7 presents the vertical profiles of the zonal shearing stress gradients in units of $kg\cdot m^{-1}\cdot s^{-2}$ per 100 mb pressure thickness, or 10^{-4}. The positive midprofile layers computed for 1800 GMT on March 8 changed sign by 1800 GMT on Mar. 9, 1969. The change in the shearing stress gradient profiles occurred with the formation of an extensive area of mountain waves over New Mexico; the stress gradients remained negative through 1800 GMT on Mar. 12, 1969.

The level of maximum wind (LMW) was used as a zero reference point for construction of the stress profiles, with layer increments of the stress gradients summed vertically above and below the level of maximum wind. The resulting profiles (fig. 8) emphasize the change in sign of the stress gradients. The arrows indicate the direction of the subgrid-scale vertical flux of zonal momentum through application of the equation

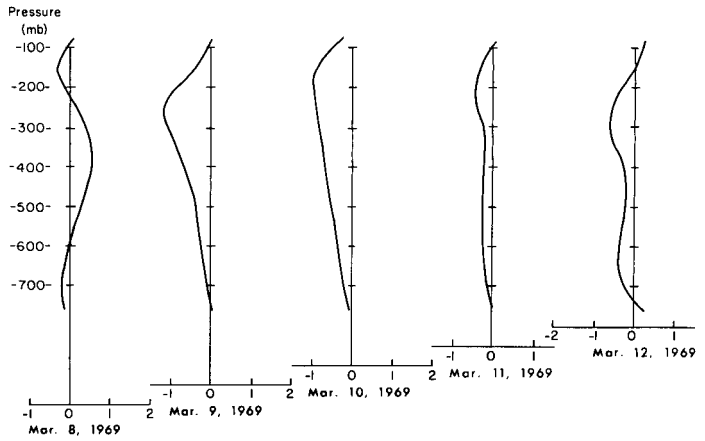

FIGURE 7.—Vertical profiles of $(\delta\bar{\tau}_x/\delta p)\,\Delta p$ in units of $kg\cdot m^{-1}\cdot s^{-2}$ per 100 mb, or $\delta\bar{\tau}_x/\delta p$ in 10^{-4}, at 1800 GMT for days indicated. The pronounced reversal of profile occurred between Mar. 8 and 9, 1969.

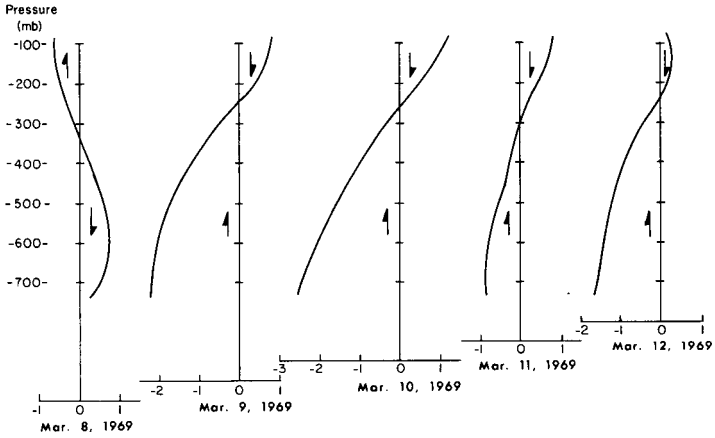

FIGURE 8.—Vertical profiles of mean stress $(\bar{\tau}_x)$ in units of $kg\cdot m^{-1}\cdot s^{-2}$ for 1800 GMT on days indicated. The directions of small-scale fluxes of zonal momentum are indicated by arrows. (Multiply by 10 to obtain $dynes\cdot cm^{-2}$.)

$$\tau_x=-\overline{\rho u'w'}. \tag{8}$$

The zero stress assumption at the LMW does not obviate the vertical convergence of zonal momentum due to stress gradients. Strong vertical convergence of zonal momentum at tropopause levels by small-scale processes dominated the profiles from March 9 through 12; vertical divergence was pronounced at the tropopause on March 8.

The stress gradients computed as residuals from eq (6) and (7), the component momentum equations, contain viscous drag forces, subgrid-scale momentum transport, and computational and data errors. Random data and computational errors were assumed held acceptably low over the large area of the region.

The individual terms in the zonal stress gradient computation for 1800 GMT on March 9 are displayed in figure 9. The pressure-gradient force term $(g\partial z/\partial x)$ nearly

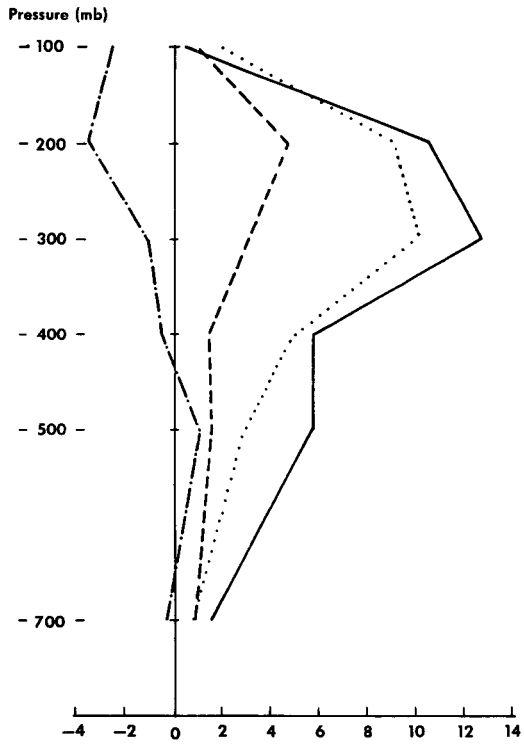

FIGURE 9.—Individual terms in the zonal stress gradient computation for 1800 GMT on Mar. 9, 1969. The dotted line is the inertial term, du/dt; dashed line is $g\partial z/\partial x$; dot-dashed line is the Coriolis term, $(-fv)$; solid line is F_x or $-g\partial\tau_x/\partial p$. Units are 10^{-4}m·s^{-2}.

balanced the Coriolis term $(-fv)$; the inertial term du/dt largely determined the magnitude and sign of F_x.

The viscous drag force can be estimated through application of the expression

$$D = -\mathbf{V}_2 \cdot \mathbf{F}_2 \tag{9}$$

where D is the viscous dissipation. If the viscous dissipation in 50 m/s flow amounts to 1W·m^{-2} in a layer 200 mb thick, the stress gradient totals 0.2 dynes·cm^{-2} (2.0×10^{-4}mb). This is two orders of magnitude smaller than the zonal stress gradients shown in figure 7 over a 200-mb layer at the tropopause on Mar. 9 and 10, 1969.

Contours of zonal stresses on isobaric surfaces shown in figures 10A and 10B exhibit the change of direction of the vertical flux of zonal momentum on the subgrid scales that took place at 700-mb between 1800 GMT on Mar. 8 and 1800 GMT on Mar. 9, 1969. The strongest downward transport on March 8 appeared over eastern New Mexico and western Texas near 35°N, 105°W at the lowest levels; the greatest upward transport occurred over the rugged terrain of central and east-central New Mexico, again at 700 mb, on March 9. One mountain peak northeast of Albuquerque, N. Mex., rises more than 4 km, and several peaks and ridges south of the city extend upward in excess of 3 km.

Table 1 presents the mean pressure and stress torques for each of seven levels for 1800 GMT on Mar. 8–12, 1969. The pressure torque was computed through the expression

$$-a\int_{p_u}^{p_l}\left[\left[\frac{\Delta z}{\Delta x}\right]_{(\lambda)}\cos\phi\right]_{(\phi)}dp \tag{10}$$

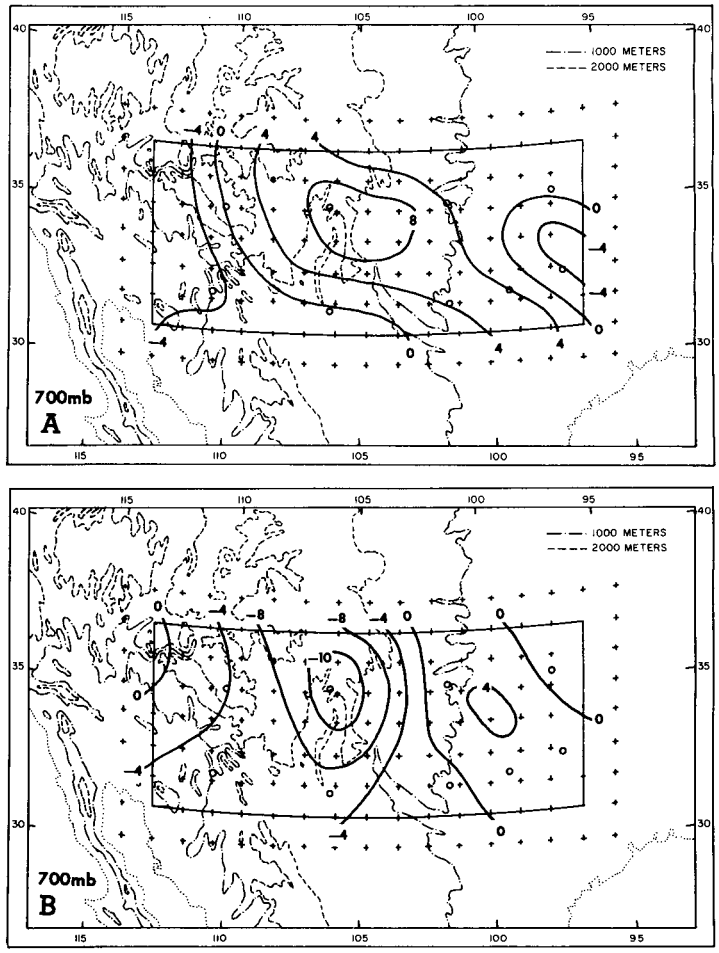

FIGURE 10.—Contours of zonal stress (τ_x) for the 700-mb level at 1800 GMT on (A) Mar. 8 and (B) Mar. 9, 1969. Units are kg·m^{-1}·s^{-2} (multiply by 10 to obtain dynes ·cm^{-2}).

and the stress torque as

$$\frac{a}{g}\int_{p_u}^{p_l}\left[\left[F_x\right]_{(\lambda)}\cos\phi\right]_{(\phi)}dp \tag{11}$$

where the subscript u defines the upper pressure boundary and the subscript l defines the lower pressure boundary of the layer. The notation $[\quad]_{(\lambda)}$ indicates a mean for all longitudes and $[\quad]_{(\phi)}$ indicates a mean for all latitudes in the computational region (Reiter 1969).

The pressure and stress torques were of the same order of magnitude and usually of opposite sign. At 1800 GMT on Mar. 9 and 10, 1969, the stress torques exhibited strong maxima near the level of maximum wind (200–400 mb).

6. KINETIC ENERGY

The large shearing stresses, earlier equated to subgrid-scale vertical momentum fluxes, suggested the action of small-scale energy mechanisms of the same order of magnitude as the synoptic scale. This prompted the investigation of the efficacy of the application of energy equations such as those used by Kung (1967, 1969) for all scales of motion in air flowing over rugged, mountainous terrain.

TABLE 1.—*Pressure torque and stress torque terms averaged over the study region on Mar. 8–12, 1969, at levels indicated. Units are 10^{3} $m^2 \cdot s^{-2}$. Times are 1800 GMT.*

Level (mb)	Pressure torque	Stress torque
	Mar. 8, 1969	
100	−0.71	0.65
150	−1.30	1.80
200	0.05	0.62
300	0.57	−1.10
400	0.98	−1.20
500	0.81	−0.53
700	0.37	0.33
	Mar. 9, 1969	
100	−0.54	0.34
150	−1.50	0.98
200	−2.10	3.40
300	−1.40	6.20
400	−0.70	3.40
500	−0.71	2.60
700	−0.33	0.65
	Mar. 10, 1969	
100	−1.10	1.00
150	−2.00	2.10
200	−2.20	1.80
300	−2.40	3.50
400	−2.00	3.40
500	−1.40	2.30
700	−0.88	1.40
	Mar. 11, 1969	
100	−0.94	0.40
150	−1.80	1.50
200	−1.80	1.90
300	−1.20	0.90
400	−0.83	1.50
500	−0.34	1.40
700	0.30	0.45
	Mar. 12, 1969	
100	−0.65	1.00
150	−0.38	0.84
200	0.03	0.78
300	1.20	3.10
400	0.82	1.20
500	1.20	1.00
700	0.57	0.90

TABLE 2.—*Summary of kinetic energy terms for Mar. 8–12, 1969. Units are 10^{-3} $m^2 \cdot s^{-3}$ or $W \cdot m^{-2}$. The estimated error for each term is appended to the total. Times are 1800 GMT.*

Level (mb)	Local change	Horizontal convergence	Vertical convergence	Generation	Dissipation
			Mar. 8, 1969		
100	−0.9	1.9	−0.5	−0.2	2.2
150	−0.4	−1.6	−1.0	4.7	2.5
200	0.8	−12.6	−1.9	17.3	2.0
300	7.0	−7.4	−0.5	18.0	3.1
400	6.6	−9.9	4.2	23.5	11.2
500	−0.4	−8.3	−0.9	12.2	3.4
700	−0.1	−1.6	−0.2	0.2	−1.5
Total	12.9±1.3	−41.9±5.9	−0.1±0.02	75.4±6.8	20.5±14.0
			Mar. 9, 1969		
100	0.9	−3.4	3.6	6.3	5.6
150	1.1	−9.3	8.4	3.3	1.3
200	−3.5	−15.4	7.6	2.9	−1.4
300	−2.1	−12.4	6.3	3.0	−1.0
400	0.0	−3.9	−1.5	8.9	3.5
500	−0.6	2.0	−5.3	2.8	0.1
700	−0.8	0.1	−1.4	−0.4	−0.8
Total	−6.0±0.6	−30.7±4.3	6.1±4.3	22.4±2.0	3.9±8.0
			Mar. 10, 1969		
100	−3.0	4.4	4.5	−9.1	2.8
150	0.5	−4.7	9.2	−6.0	−2.0
200	0.3	−18.3	5.4	−4.7	−17.9
300	−2.9	2.1	−3.1	−9.2	−7.3
400	−1.4	9.2	−2.9	−10.3	−2.6
500	−0.2	4.0	−3.0	−5.5	−4.3
700	0.4	0.8	−0.7	0.9	0.6
Total	−5.2±0.5	4.8±0.7	−0.8±0.2	−37.3±3.4	−28.0±4.8
			Mar. 11, 1969		
100	−0.8	−8.0	4.2	4.2	1.2
150	−1.8	−2.6	9.2	3.9	12.3
200	−5.2	−24.4	13.7	13.7	8.2
300	−13.3	−13.5	−15.4	12.4	−3.2
400	−2.7	−10.3	−4.2	2.5	−9.3
500	−1.0	−2.2	1.7	0.1	0.6
700	−0.5	−0.5	0.7	1.6	2.3
Total	−23.5±2.4	−51.8±7.2	1.2±0.2	32.2±2.9	5.3±10.7
			Mar. 12, 1969		
100	−7.3	7.4	−15.1	13.1	12.7
150	1.6	−6.0	−6.7	15.0	0.7
200	9.5	−7.3	12.0	3.9	−0.9
300	7.0	−1.2	5.6	1.1	−1.5
400	3.1	−3.7	2.2	3.3	−1.3
500	0.4	−6.4	0.8	5.8	−0.2
700	−0.5	−1.4	−0.3	1.6	0.4
Total	14.0±1.4	−21.7±3.0	6.6±1.1	32.9±3.0	3.7±8.5

Frictional dissipation was not calculated directly because of the apparent substantial vertical fluxes by gravity waves. Rather, dissipation was computed as a residual in the kinetic energy budget in the form:

$$-D=-\frac{A}{g}\int_{p_u}^{p_l}\left[\frac{\partial K}{\partial t}\right]_{(\phi,\lambda)}dp-\frac{L}{g}\int_{p_u}^{p_l}[Kc_n]_{(L)}dp+\frac{A}{g}\{[K\omega]_{(\phi,\lambda),p_u}-[K\omega]_{(\phi,\lambda),p_l}\}-A\int_{p_u}^{p_l}[\mathbf{V}_2\cdot\nabla z]_{(\phi,\lambda)}dp \quad (12)$$

where $[\ ]_{(\phi,\lambda)}$ indicates an area average; $[\ ]_{(L)}$, an average over the perimeter; $[\ ]_{(\phi,\lambda),p_l}$, an area average at the lower pressure boundary; and $[\ ]_{(\phi,\lambda),p_u}$, an area average at the upper pressure boundary. The flow normal to the perimeter, c_n, is positive outward; K is the kinetic energy, $(u^2+v^2)/2$, per unit mass; $\mathbf{V}_2$ is the two-dimensional velocity vector, z is the height above MSL, ω has the usual definition, $\omega=dp/dt$, and A is the total area. The ω calculation utilized the equation of continuity in isobaric coordinates (i.e., $\nabla_p\cdot\mathbf{V}_2=-\partial\omega/\partial p$) with the assumption that $[\omega]_{(\phi,\lambda),p_u}\doteq 0$ at 75 mb, and integrating

TABLE 3.—*Frictional dissipation in the free atmosphere (positive when kinetic energy is transformed to internal energy)*

Author	Layer	W·m^{-2}
Kung (1969)	750– 70 mb	2. 28
	25, 000–40, 000 ft	1. 28
Trout and Panofsky (1969)	25, 000–40, 000 ft	1. 32
Ellsaesser (1969)	700– 100 mb	1. 44
Holopainen (1963)	900– 200 mb	6. 2
Jensen (1961)	925– 100 mb	0. 92
(*) This study	775– 75 mb	1. 09

downward to the lowest levels. The first term on the right-hand side represents the local change of kinetic energy with time; the second, the horizontal convergence of kinetic energy; the third, the synoptic scale vertical convergence of kinetic energy; and the last term, the generation of kinetic energy within the boundaries.

The assumption of $\omega=0$ at 75 mb was considered less stringent than that of $w=0$ due to the low density of the atmosphere at 75 mb. Profiles of kinetic energy for all pressure levels at each gridpoint enabled the selection of K at layer interfaces; $K\omega$ represented point values at the interfaces. From these point values, $[K\omega]_{(\phi,\lambda)}$ and the third term on the right-hand side of eq (12) were evaluated from each layer at each time period.

The results of applying the kinetic energy equation in pressure coordinates to the volume are presented in table 2 for 1800 GMT on Mar. 8–12, 1969. Generation on March 8 proved extremely large when compared to long-term means (Kung 1967), occurring through a deep layer from 175 to 600 mb. The generation rate diminished by 1800 GMT on March 9, with a maximum again at 400 mb, becoming negative, except for the lowest layer, by 1800 GMT on March 10. The level of maximum generation occurred at 200 mb on March 11 and at 150 and 500 mb on March 12.

The (residual) dissipation rate changed markedly with time, ranging from over 20 W·m^{-2} on March 8 to a negative dissipation rate of 28 W·m^{-2} on March 10. When dissipation is positive, kinetic energy is being transformed to internal energy. A discussion and interpretation of the phenomenon is made later in this paper on the basis of gravity wave propagation and energy storage. If an average over the volume for all days is taken, a mean dissipation of 1.1 W·m^{-2} follows.

For comparison with the values computed here, table 3 indicates a range of values for frictional dissipation in the atmosphere above the boundary layer. Values by Kung (1969) are for the annual mean, and are presented in two layer thicknesses; values computed by Trout and Panofsky (1969) are for the upper troposphere. The value indicated by (*) is an average over time of this dissipation computed here as a residual of the kinetic energy equation [eq (12)].

7. INTERPRETATION OF COMPUTATIONAL RESULTS

The abrupt reversal in the direction of the subgrid-scale vertical flux of zonal momentum, as indicated by computed shearing stresses, accompanied the appearance of large areas of wave structure photographed during the Apollo 9 flight on Mar. 9, 1969. Unfortunately, no cloud pictures were taken March 10, but photographs of the southwestern United States on March 11 and 12 indicated that the wave population had diminished prior to 1800 GMT on Mar. 11, 1969. The life cycle of the wave population can be viewed as paralleling an "energy generation cycle" exhibited in table 2, suggesting a relationship between the subgrid-scale waves and the synoptic scale energy budgets.

The stably stratified atmosphere over the southwestern United States on Mar. 8, 9, and 10, 1969, contained substantial shears in the upper half of the tropopause, effectively preventing upward turbulent vertical flux of zonal momentum by eddy mixing. In such regions, where eddy turbulent momentum transport is inhibited, the transfer may plausibly be fulfilled by internal waves (Stewart 1969).

The gravity-wave model developed by Eliassen and Palm (1961) provides a mechanism for the vertical transport of momentum and energy. The model assumed a vertical shear of the horizontal wind, a nonuniform basic current, and wave motion constrained to act in the x-z plane. The wave equation becomes

$$\frac{\partial}{\partial x}(EU+pu')+\frac{\partial}{\partial z}(pw')=-\rho_o\frac{\partial U}{\partial z}u'w' \qquad (13)$$

where U is the mean flow velocity, ρ_0 is the equilibrium density, u' and w' are the perturbation velocities in the x and z directions, respectively, p is pressure, and E is the total wave energy per unit volume.

The right-hand side of eq (13) represents a source of wave energy through the conversion of kinetic energy of the mean current and can be either positive or negative. Multiplying the perturbation zonal momentum equation

$$\rho_o U\frac{\partial u'}{\partial x}+\rho_o\frac{U\partial}{\partial z}w'+\frac{\partial p}{\partial x}=0 \qquad (14)$$

by $(\rho_0 Uu'+p)$ and integrating over x from $-\infty$ to $+\infty$ results in

$$\int_{-\infty}^{+\infty}pw'dx=-U\rho_o\int_{-\infty}^{+\infty}u'w'dx; \qquad (15)$$

integration of eq (13) with respect to x from $-\infty$ to $+\infty$ yields

$$\frac{d}{dz}\int_{-\infty}^{+\infty}pw'dx=-\frac{\partial U}{\partial z}\rho_0\int_{-\infty}^{+\infty}u'w'dx \qquad (16)$$

for the case of lack of resonance.

Thus, in a layer in which $U\neq 0$, the vertical flux of energy, $\int_{-\infty}^{+\infty}pw'dx$, varies with height in proportion to U; sources of wave energy vary with height in proportion to $\partial U/\partial z$. Further, if U is everywhere positive in the layer, the vertical flux of energy takes a direction opposite to the vertical flux of momentum; that is, if energy is transferred downward, momentum flows upward by wave action.

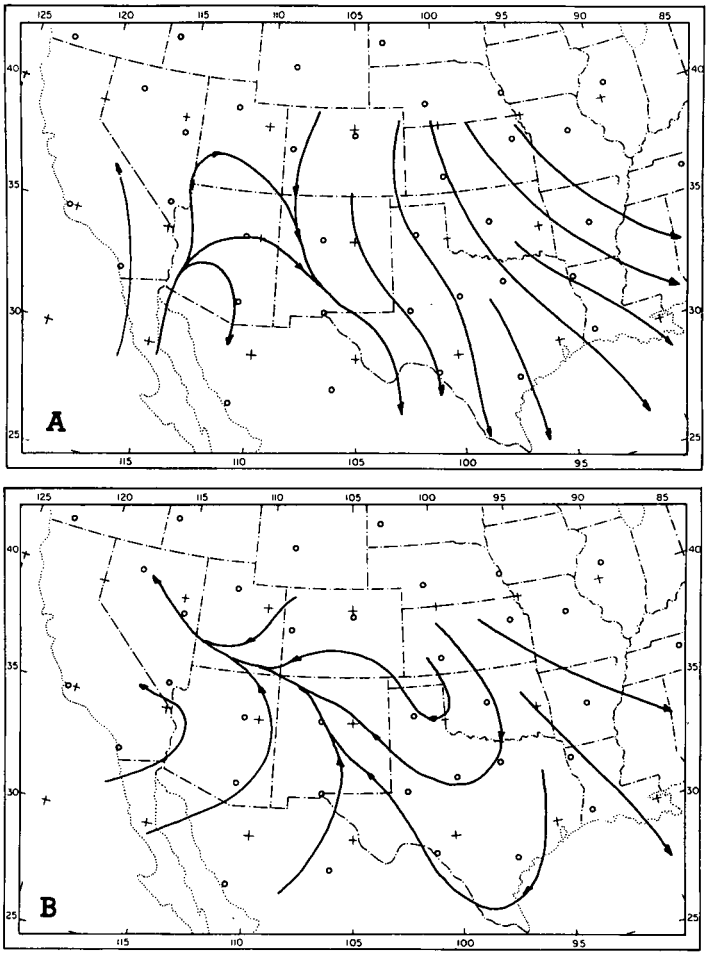

FIGURE 11.—Streamline analyses for flow in the lowest 100 mb of the atmosphere at 0000 GMT on (A) Mar. 9 and (B) Mar. 10, 1969.

In Fourier representation, it can be shown that, where $U<<\gamma^{-1/2}$ for a single component in mountain waves with $U\neq 0$ and $\gamma \equiv d\rho/dp$,

$$\overline{pw'}=\frac{U\rho_0}{k^2}\overline{\frac{\partial w'}{\partial x}\frac{\partial w'}{\partial z}} \tag{17}$$

where k is the wave number and vertical energy transport depends upon the tilt of the waves with height. If the wave axis tilts downstream with increasing height, perturbation energy flows downward and momentum upward; if U increases with height, the kinetic energy of the wave motion converts into mean motion. Conversely, if the axis tilts upstream with increasing height, perturbation energy flows upward, momentum downward, and kinetic energy of mean motion converts to wave energy.

The downstream tilt with height of the wave axis is compatible with easterly air flow in the lower levels and westerly flow at upper troposheric levels; upstream tilt occurs with westerly flow extending upward from the surface layers. The streamline analysis of planetary boundary-layer winds (fig. 11A) for 0000 GMT on Mar. 9, 1969, exhibits the westerly flow typical of upstream tilt; the analysis for 0000 GMT on Mar. 10, 1969, shows the contrasting easterly flow in the lowest 100 mb of the atmosphere over western Texas and New Mexico (fig. 11B). The easterly boundary-layer flow corresponded to a negative zonal shearing stress in the atmosphere (upward momentum transfer); westerly flow at 0000 GMT on March 9, preceding the reversal of direction of vertical momentum flux, corresponded to a positive zonal shearing stress (downward momentum transfer).

Zonal shearing stresses in the atmosphere at the top of the planetary boundary layer averaged as high as 25 dynes·cm^{-2} (25×10^{-3}mb) on occasion, when measured in a pressure coordinate system. Local values over the high mountains in central and east-central New Mexico reached as much as four times the average.

Blumen (1965), using a wave model for airflow over a line of equally spaced circular mountains, computed a surface stress of 16 dynes·cm^{-2} (16×10^{-3}mb) with a wave amplitude of 300 m. Since the stress due to wave drag increases according to the square of the amplitude, an amplitude of about 800 in the same model would approximate the stress computed over central New Mexico at 1800 GMT on Mar. 10, 1969.

The role of internal gravity waves in the energy cycle was investigated through a calculation of the buoyant potential energy stored in the density variations of the waves. If the mean density distribution is statically stable, the action of vertical motions against buoyant forces can act as a sink on the subgrid scale to the energy of the mean and turbulent flow.

The removal of energy from a turbulent flow field and the transformation of that energy has been treated by Bolgiano (1962); he assumed adiabatic processes in developing the equations of motion for mountain-perturbed flow with stable stratifications. Bolgiano introduced potential density ($\rho=p/R\theta$) and density-normalized pressure in developing an expression for the storage of potential energy due to the vertical displacement of fluid elements against the force of gravity. Per unit mass, this potential energy storage is

$$\phi=-\frac{1}{2}\frac{g(\rho')^2}{\rho_0}\left(\frac{d\bar{\rho}}{dz}\right)^{-1} \tag{18}$$

where $d\bar{\rho}/dz$ represents the vertical gradient of the mean potential density; ρ' is the density deviation from the base density ρ_0.

An approximation of the amount of potential energy contained in the density deviations of a wave population requires (1) an estimate of the areal coverage of the waves, (2) a knowledge of atmospheric stabilities in the wave region, and (3) reasonable estimates of the wave amplitudes.

The Apollo 9 photographs serve to give a first-order estimate of the wave population over western Texas and New Mexico. The area ABCFED in figure 4 exhibits wave structure at two levels. Longer lee waves at A in figure 12 extend downstream from the jet stream cloud into western Texas where they appear at A in figure 13. Billow clouds with a wavelength of about 500 m are superimposed on the longer waves at B and upstream toward A in the same picture. Cap clouds frequently existed over individual ridges such as at B in figure 12.

The Apollo 9 photographic coverage amounted to about 41 percent of the computational area at approxi-

456-793 O - 72 - 2

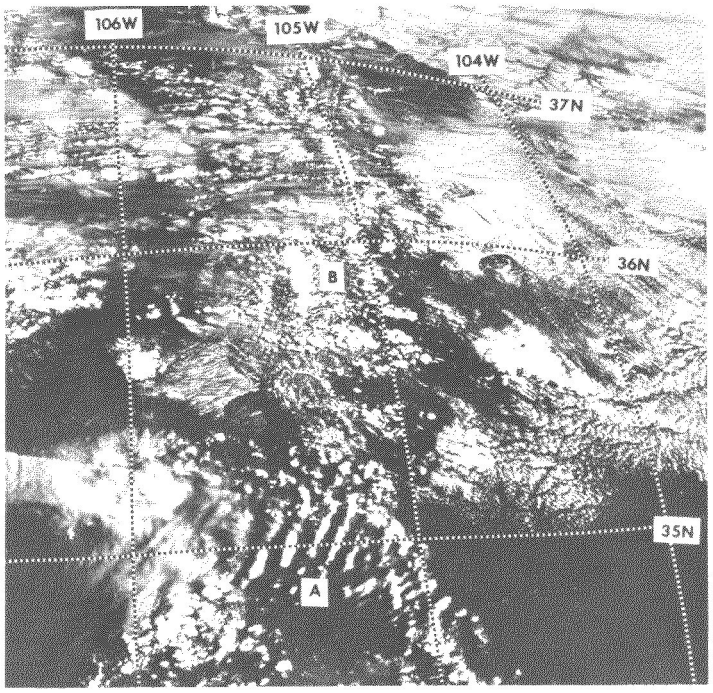

FIGURE 12.—Apollo 9 photograph (No. 3447) taken at approximately 1804 GMT on Mar. 9, 1969. Lee wave clouds are visible at A; a cap cloud covers the mountain ridge at B.

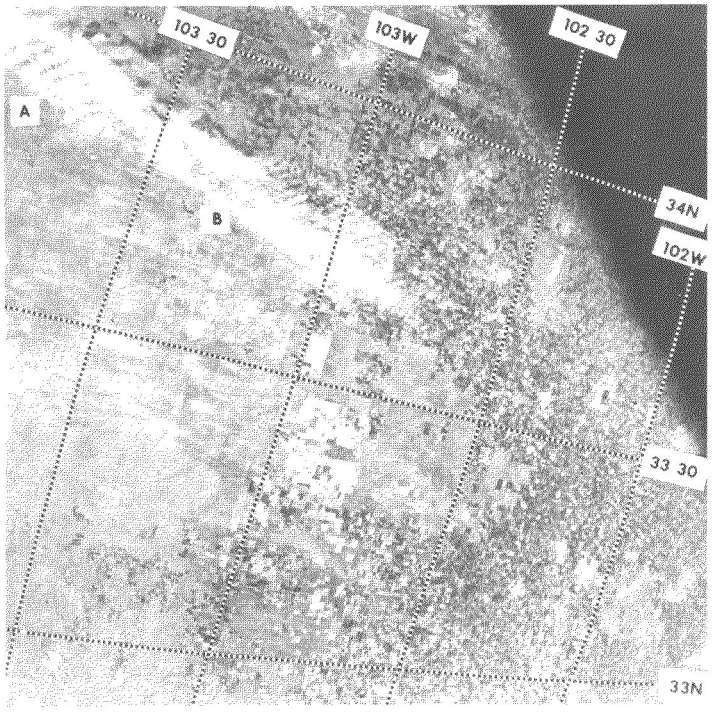

FIGURE 13.—Apollo 9 photograph (No. 3294) taken at approximately 1804 GMT on Mar. 9, 1969. Wave clouds at A are to the lee of the mountains; billows at B are superimposed on the longer waves.

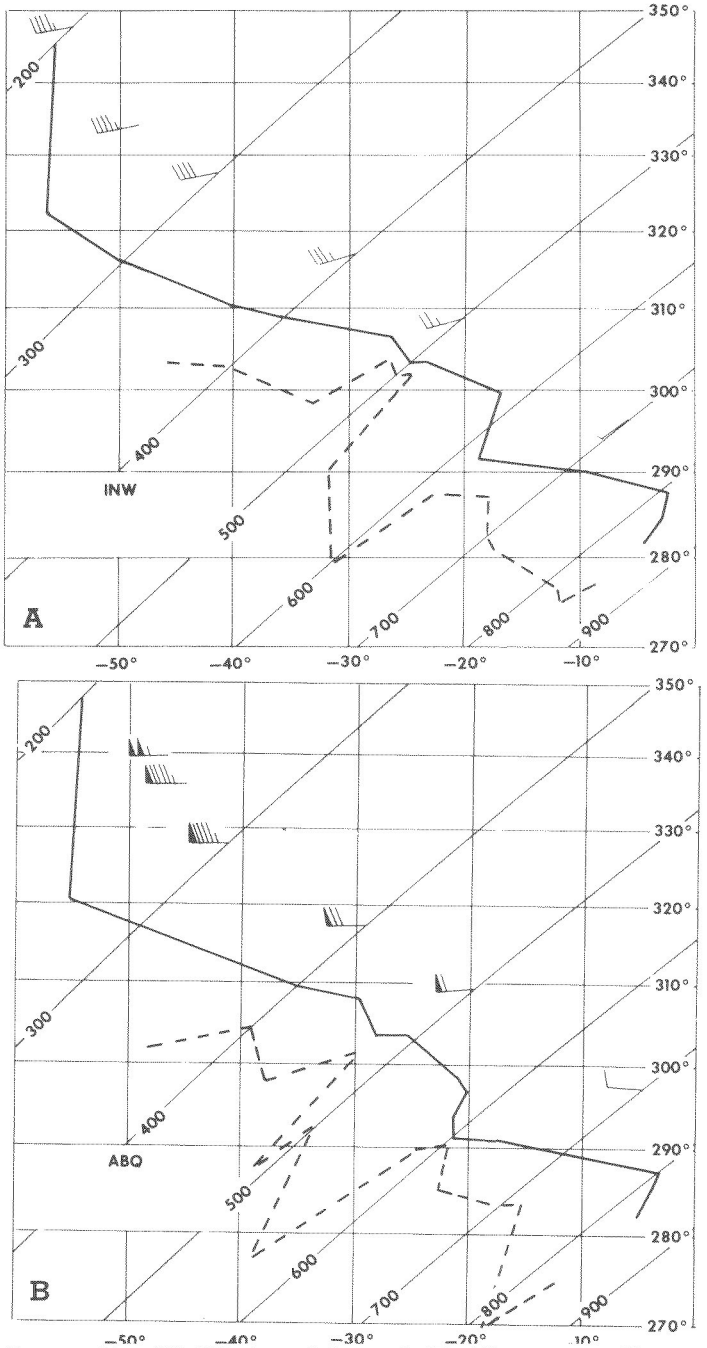

FIGURE 14.—(A) Winslow, Ariz., and (B) Albuquerque, N. Mex., soundings for 1200 GMT on Mar. 9, 1969. Solid line is temperature (°C); dashed line is the dew-point temperature (°C). Wind barbs indicate velocity in kt.

mately 1800 GMT on Mar. 9, 1969, with an average cloud cover of 28 percent of the area pictured; roughly 30 percent of the clouds revealed wave structure. Much of the region showed the same stable layers as found in the Winslow, Ariz., and Albuquerque, N. Mex. (figs. 14A and 14B) soundings. Only in the southeastern sector were stable layers absent from the soundings. In view of the cap clouds, and because of the extensive sheets of stable layers imbedded in the nearly uniform flow at midtropospheric levels, a reasonable estimate of the areal extent of waves would be 30 percent.

Wavelengths varied from the 500-m billows to the 8-km lee waves. All wavelengths were assumed to be within the range over which buoyant forces act since there appears to be no definite upper limit for the "buoyant subrange" of wave disturbances (Lin et al. 1969).

The amplitude of the waves probably ranged from

TABLE 4.—*Energy residual over the computational region*

Layer center	Residual
(mb)	(W·m^{-2})
100	5. 6
150	4. 1
200	−3. 0
300	−3. 2
400	−2. 4
500	−0. 9
700	0. 6

typical values of 100–200 m for the billows (Woods 1969) to 2 or 3 km over mountain ridges where cap clouds formed in relatively dry air. Typical lee waves have a total vertical displacement of 1 km (Vergeiner and Lilly 1969). For the computations described here, a mean vertical displacement of 350 m was assumed, corresponding to the typical lee wave, and the Winslow and Albuquerque soundings for 1200 GMT on March 9 (approx. 6 hr prior to the photographic mission for Apollo 9 for that day) were selected for potential-energy calculations. An examination of the moisture available in the stable layers at Albuquerque indicated a required lifting of about 200 m for condensation.

The Winslow and Albuquerque soundings were divided into several layers having uniform lapse rates, and eq (18) was applied to each layer from 800 mb to the tropopause. The computed potential energy in the wave structure totaled 6.7×10^5 J·m^{-2} at Winslow and 9.3×10^5 J·m^{-2} at Albuquerque, or an average of 8.0×10^5 J·m^{-2}. The 21 W·m^{-2} indicated as an energy residual at 1800 GMT on March 8 could supply the 8.0×10^5 J for 30 percent of the study region in a period of 3.2 hr.

The amplitudes of internal gravity waves will continue to grow as long as energy is supplied, until the wave motion becomes potentially unstable. Once instability occurs, patches of turbulence will result in loss of energy through viscous dissipation to heat (Phillips 1967). If energy is no longer continuously supplied to the internal gravity waves, the motion will remain stable.

An average over area and time of the residual in the kinetic energy calculation might be expected to yield a reasonable rate of energy dissipation to heat at each level in the atmosphere if no systematic vertical redistribution of energy takes place. Table 4 gives the average value of the residual for 1800 GMT on March 9–12 in W·m^{-2}.

An excess of kinetic energy appears at 100 and 150 mb, and a deficiency from 200 to 500 mb. The apparent vertical distribution requirement of the energy residual might be attributed to a vertical transport by the subgrid-scale gravity waves, unaccounted for in the ω calculation on the larger scale. While the kinematic method of calculating the vertical pressure velocity is often credited with substantial random errors, there is no reason to believe that systematic negative energy residuals such as those shown in table 4 would result from the application of the kinematic method.

8. SUMMARY

A series of pictures taken from the earth-orbiting Apollo 9 spacecraft provided wide coverage of cloud features for Mar. 8, 9, 11, and 12, 1969. The high-resolution handheld camera photographed extensive areas of wave structure in cloud layers over Arizona, New Mexico, and western Texas. Long cumulus streets and cirrus streaks in the pictures closely approximated the wind directions recorded by conventional meteorological devices and augmented the rawinsonde and pilot ballon wind data in mesoscale detail. The wave structure and the cumulus rows were undetected by the higher-flying weather satellites due to the coarse resolution of the ESSA vidicon cameras.

Zonal shearing stress gradients, measured as residuals in the u-component momentum equation, attained values of a few tens of dynes·cm^{-2}(10^{-3}mb) over the rugged, irregular terrain of central New Mexico. On March 8, the stress gradients indicated a subgrid-scale vertical flux divergence of zonal momentum from the level of maximum wind. On March 9, and for the remaining period until March 12, the stress gradients were contradirectional to those of March 8, with a change to vertical flux convergence into upper troposphere and tropopause levels.

The zonal wind velocities in the upper troposphere and lower stratosphere increased sharply with the onset of strong subgrid-scale vertical flux convergence of zonal momentum at those levels. The countergradient flux of zonal momentum coincided with a change of low-level flow from westerlies to easterlies over and east of the mountains, suggesting a downwind tilt with height of the vertical wave axes. Mean values of the energy budget residual at standard levels indicated a flux of kinetic energy downward into the lower troposphere when zonal momentum was transported upward.

Based on Apollo 9 photographs, the areal coverage of gravity waves over the computational region was estimated at 30 percent. Winslow, Ariz. and Albuquerque, N. Mex. soundings at 1200 GMT on March 9 were used to calculate the buoyant potential energy contained in the density deviations of the waves. This energy totaled 8×10^5 J·m^{-2} in the wave area below the tropopause for an estimated mean particle displacement of 350 m. While the estimation of this energy could be in error by a factor of two or three, the energy sink in the extensive wave population was of the same order of magnitude as the synoptic scale energy generation and divergence.

Through the action of large areas of gravity waves with a downstream tilt of their vertical axes, a substantial countergradient flux of zonal momentum can converge at the tropopause to maintain or increase tropopause-level flow against frictional dissipation to heat. The buoyant potential energy contained in extensive gravity-wave populations can be large enough to act as an energy sink of the same order of magnitude as the synoptic scale kinetic energy generation.

REFERENCES

Blumen, William, "A Random Model of Momentum Flux by Mountain Waves," *Geofysiske Publikasjoner*, Vol. 26, No. 2, Oslo, Norway, Feb. **1965**, 33 pp.

Bolgiano, Ralph, Jr., "Structure of Turbulence in Stratified Media," *Journal of Geophysical Research*, Vol. 67, No. 8, July **1962**, pp. 3015–3023.

Eliassen, Arnt, and Palm, Enok, "On the Transfer of Energy in Stationary Mountain Waves," *Geofysiske Publikasjoner*, Vol. 22, No. 3, Oslo, Norway, Sept. **1961**, 23 pp.

Ellsaesser, Hugh W., "A Climatology of Epsilon (Atmospheric Dissipation)," *Monthly Weather Review*, Vol. 97, No. 6, June **1969**, pp. 415–423.

Fowler, Alan H., and Wilson, Charles W., "Cubic Spline, a Curve Fitting Routine," *Report* No. Y–4100, Revision 1, Union Carbide Corp., Nuclear Division, Oak Ridge, Tenn., Apr. 21, **1966**, 109 pp.

Fritsch, J. Michael, "Objective Analysis of a Two Dimensional Data Field by the Cubic Spline Technique," *Atmospheric Science Paper* No. 143, Colorado State University, Fort Collins, Aug. **1969**, 34 pp.

Gilman, Peter A., "On the Vertical Transport of Angular Momentum in the Atmosphere," *Pure and Applied Geophysics*, Vol. 57, No. 1, Basel, Switzerland, Jan. **1964**, pp. 161–166.

Haurwitz, Bernhard, *Dynamic Meteorology*, McGraw-Hill Book Co., Inc., New York, N.Y., **1941**, 365 pp. (see pp. 114–124).

Holopainen, Eero O., "On the Dissipation of Kinetic Energy in the Atmosphere," *Tellus*, Vol. 15, No. 1, Stockholm, Sweden, Feb. **1963**, pp. 26–32.

Jensen, Clayton E., "Energy Transformation and Vertical Flux Processes Over the Northern Hemisphere," *Journal of Geophysical Research*, Vol. 66, No. 4, Apr. **1961**, pp. 1145–1156.

Kung, Ernest C., "Diurnal and Long-Term Variations of the Kinetic Energy Generation and Dissipation for a Five-Year Period," *Monthly Weather Review*, Vol. 95, No. 9, Sept. **1967**, pp. 593–606.

Kung, Ernest C., "On the Momentum Exchange Between the Atmosphere and Earth Over the Northern Hemisphere," *Monthly Weather Review*, Vol. 96, No. 6, June **1968**, pp. 337–341.

Kung, Ernest C., "Further Study on the Kinetic Energy Balance," *Monthly Weather Review*, Vol. 97, No. 8, Aug. **1969**, pp. 573–581.

Lester, Peter F., "A Study on the Structure and Behavior of Jet Streams Over the Western United States," *Technical Report*, Contract No. E–10–68G, Department of Atmospheric Science, Colorado State University, Fort Collins, June **1969**, 115 pp.

Lin, J. T., Panchev, S., and Cermak, J. E., "A Modified Hypothesis on Turbulence Spectra in the Buoyancy Subrange of Stably Stratified Shear Flow," *Radio Science*, Vol. 4, No. 12, Dec. **1969** pp. 1333–1337.

Lorenz, Edward N., "The Nature and Theory of the General Circulation of the Atmosphere," *WMO Bulletin*, Vol. 16, No. 2 World Meteorological Organization, Geneva, Switzerland, Apr. **1967**, pp. 74–78.

Oort, Abraham H., and Rasmusson, Eugene M., "On the Annual Variation of the Monthly Mean Meridional Circulation," *Monthly Weather Review*, Vol. 98, No. 6, June **1970**, pp. 423–442.

Palmén, Erik, "On the Interhemispheric Mass Circulation Across the Equator," *Quarterly Journal of the Royal Meteorological Society*, Vol. 92, No. 1, London, England, Jan. **1966**, pp. 157–158.

Palmén, Erik, and Newton, Chester W., *Atmospheric Circulation Systems: Their Structure and Physical Interpretation*, Academic Press, New York, N.Y., June **1969**, 603 pp. (see pp. 11–22, 286, 442, 564–568).

Phillips, O. M., "On the Bolgiano and Lumley-Shur Theories of the Buoyancy Subrange," *Proceedings of the Colloquium on Atmospheric Turbulence and Radio Wave Propagation, Moscow, U.S.S.R., June 15–22, 1965*, Izdatvo Nauka, **1967**, 374 pp. (see pp. 121–129).

Priestley, Charles Henry Brian, *Turbulent Transfer in the Lower Atmosphere*, The University of Chicago Press, Chicago, Ill., **1967***a*, 130 pp.

Priestley, Charles Henry Brian, "On the Importance of the Variability in the Planetary Boundary Layer," *Report of the Study Conference of the Global Atmospheric Research Programme, Stockholm, Sweden, June 28–July 11, 1967*, Appendix IV, International Union of Geodesy and Geophysics, Toronto, Canada, **1967***b*, 4 pp.

Reiter, Elmar R., *Atmospheric Transport Processes, Part I: Energy Transfers and Transformations*, U.S. Atomic Energy Commission, Division of Technical Information, Oak Ridge, Tenn., **1969**, 253 pp. (see pp. 20–27).

Reiter, Elmar R., and Foltz, Harry P., "The Prediction of Clear Air Turbulence Over Mountainous Terrain," *Journal of Applied Meteorology*, Vol. 6, No. 4, June **1967**, pp. 549–556.

Rossby, Carl Gustav, "On the Vertical and Horizontal Concentration of Momentum in Air and Ocean Currents: I. Introductory Comments and Basic Principles, With Particular Reference to the Vertical Concentration of Momentum in Ocean Currents," *Tellus*, Vol. 3, No. 1, Stockholm, Sweden, Feb. **1951**, pp. 15–27.

Starr, Victor P., *Physics of Negative Viscosity Phenomena*, McGraw-Hill Book Co., Inc., New York, N.Y., **1968** 256 pp.

Starr, Victor P., and Dickinson, Robert E., "Large Scale Vertical Eddies in the Atmosphere and the Energy of the Mean Zonal Flow," *Geofisica Pura e Applicata*, Vol. 55, No. 2, Milan, Italy, Mar. **1963**, pp. 133–136.

Stewart, Robert W., "Turbulence and Waves in a Stratified Atmosphere," *Radio Science*, Vol. 4, No. 12, Dec. **1969**, pp. 1269–1278.

Trout, Dennis D., and Panofsky, Hans A., "Energy Dissipation Near the Tropopause," *Tellus*, Vol. 21, No. 3, Stockholm, Sweden, June **1969**, pp. 355–358.

Vergeiner, Ignatz, and Lilly, Douglas K., "The Dynamic Structure of Lee Wave Flow as Obtained From Balloon and Aircraft Observations," *NCAR Manuscript* No. 69–115, National Center for Atmospheric Research, Boulder, Colo., July **1969**, 22 pp.

Woods, J. D., "On Richardson's Number as a Criterion for Laminar-Turbulent-Laminar Transition in the Ocean and in the Atmosphere." *Radio Science*, Vol. 4, No. 12, Dec. **1969**, pp. 1289–1298.

[Received March 5, 1971; revised September 27, 1971]